Thermo-Mechanical Properties and Stress-Strain Curves of Ordinary Cementitious Mortars at Elevated Temperatures

Patrick Bamonte[1], Pietro G. Gambarova[1] and Francesca Sciarretta[2]

[1] Politecnico di Milano, Piazza Leonardo da Vinci 32, 20133 Milan, Italy

[2] IUAV – University of Architecture of Venice, Dorsoduro, Venice, Italy

ABSTRACT

The mechanical behaviour of three bed-fixing mortars (one *reference cement-lime mortar*, cube strength ≈ 5 MPa and two *cement mortars*, cube strength ≈ 10 and 15 MPa) is investigated in this project in ordinary conditions and after being heated to 200, 400 and 600°C, and up to 900°C to evaluate the thermal diffusivity. The objectives of this study are two: (a) to extend the database on the high-temperature behaviour of ordinary cementitious mortars; and (b) to develop stress-strain relationships as a function of the temperature, that may be useful in the formulation of macro finite elements for masonry structures.

On the whole, the heat-induced mechanical decay of the cementitious mortars investigated in this study (a) agrees with the experimental results available in the literature and (b) is very similar to that of ordinary concrete, as far as it concerns the compressive strength, tensile strength and elastic modulus. Compared to concrete at high temperatures, however, the mass loss in the mortars is higher, the thermal diffusivity is always smaller and the softening branch of the stress-strain curves indicates a definitely higher ductility.

The test results allow calibrating an analytical stress-strain law in compression. The formulation is derived from that provided by Eurocode 2 for concrete at high temperature, but accounting for the smaller elastic modulus, the greater ductility and the gentler softening of the mortars at any temperature.

Keywords: cementitious mortars, high temperature, fire, compressive/tensile strength, modulus of elasticity, density, thermal diffusivity, stress-strain relationship

1. INTRODUCTION

Mortars are well-known construction materials whose introduction goes back to the 19th century for cement-lime and cement mortars (commonly used in modern buildings and in the refurbishment of existing buildings) and to centuries or even millennia ago for lime and lime-pozzolanic mortars (commonly found in historic masonry) [1].

According to the performance-based standard EN 998-2 [2], masonry mortars can be classified on the grounds of the compressive strength, into six classes (M1, M2.5, M5, M10, M15 and M20). As well, mortars can be subdivided on the basis of the type of binder(s), i.e. aerial lime, hydraulic lime, cement, double-binder (e.g. cement and hydraulic lime, or gypsum and aerial lime) and gypsum. Sand is generally twice the amount of binder; the water content, of which 0.5 is a typical value, can significantly affect the fire performance [3]. In contemporary mortars, the most used binders are Portland cement (introduced in the late 19th Century) and hydraulic lime. In the majority of ancient masonry structures that have survived until our times, hydraulic-lime mortars have allowed for structural robustness and durability. Slaked lime and, in very dry climates, gypsum are also found in traditional mortars [4], while pozzolanic components have been used both in traditional and contemporary mortars (pumice ashes in the former case and zeolite or silica fume in the latter, replacing about the 30% of aerial lime or the 10% of the cement [5]). Pozzolanic mortars generally have higher strength and better durability (thanks to improved resistance to the attack of chlorides and sulfates) than normal mixes.

Today, more than in the past, Fire Safety and Structural Fire Design require the physical and mechanical decay of cementitious mortars to be fully understood with reference to high-temperature environments, all the more because ordinary mortars are used in a variety of structural and non-structural members [6].

In the last decades, several research projects and papers have been focused on the high-temperature behaviour of mortars, but there is still need for further experimental evidence concerning cement-lime mortars and cement mortars, during a fire and after cooling down to room temperature (*residual conditions*). Contributions in this field would facilitate the formulation of reliable temperature-dependent stress-strain laws, and would improve the modelling of masonry structures exposed to fire. Mortar layers should not be the *weakest link of the resisting chain*, see – for instance – the firewall in Figure 1 [7].

Figure 1. Concrete-block firewall past a fire: thermal bowing towards the reader and extensive detachment of the front sheet of the blocks (from [7], by courtesy of the Headquarters of the National Corps of Firemen, Turin, Italy).

Up to the beginning of our millennium, the interest for the high-temperature behaviour of cementitious mortars has been very limited, as confirmed by the comprehensive and highly informative paper by Tate [8], where none of the 45 references is about cement/lime mortars exposed to high temperatures and fire. After 2005, however, thanks to the increasing technical and scientific interest for high-performance (f_c = 30-60 MPa) and ultra high-performance mortars and cementitious pastes (f_c > 90 MPa), not only many papers have been dedicated to this subject, but also lime, cement-lime and cement mortars (*ordinary mortars*) have enjoyed a renewed attention, with specific reference to high temperatures.

In a similar way to other cementitious materials (like concrete [9]), many are the causes of the sizeable, and mostly unrecoverable, mechanical decay occurring in cementitious mortars, during and after a thermal process [10-12]:

(a) evaporation of the free water (capillary water, above 100°C);
(b) expulsion of the gel water above 150°C;
(c) decomposition of gypsum into calcium sulphate and water (130-170°C);
(d) expulsion of the chemically-bound water (from aluminous and ferrous constituents) above 250°C;
(e) decomposition of calcium silicate hydroxides above 400°C;
(f) dissociation of calcium hydroxide into calcium oxide and water at 470°C;
(g) expansive inversion of α- to β-quartz at 573°C in siliceous aggregate, and
(h) calcination above 700°C.

Strength increases, however, are possible below 400°C because of the compaction of the cement gel layers following the expulsion of free water [12].

Because of the previously described phenomena, the compressive strength of mortars increases up to 600°C in lime-pozzolanic mortars containing a limited amount of cement (natural pozzolan and white cement [13]), remains almost constant up to 400°C in cement-lime mortars [14,15], decreases almost linearly in cement mortars (-40% at 500°C in [16]), and strongly decreases in cement-pozzolanic mortars (more with fly ash and silica fume, less with pumice [17]). Adding graphite [18] or using blended cement [12] tends to improve the compressive strength up to 300°C. At higher temperatures, strength decreases with a loss in excess of 50% above 600°C, but earlier decreases may occur (> 300°C in [12]). However, partially replacing ordinary Portland cement with fly ash [19] or with a combination of silica fume and metakaolin markedly increases mortar residual strength (up to 800°C [20]).

The previous considerations hold for both *hot conditions* [14-16,21] and *residual conditions* [12,13,17,18,20,21], with the tests carried out at high temperature and past cooling, respectively. Note that the compressive strength in ordinary conditions spans from 4.5-16 MPa in [13-15,20] to 35-45 MPa in [17,18] and 55-60 MPa in [11,12,16].

The elastic modulus of cementitious mortars exhibits a monotonic decrease at increasing temperatures, and loses more than 50% of its original value at 500°C [14,15,18] (and even more, like 80% at 400°C [13] or 90% at 500°C [16]). The elastic modulus is, therefore, more heat-sensitive than the compressive strength, as well-known in concretes, but may even slightly increase after cooling ([22,23], T_{max} = 300°C).

As for tension, the indirect tensile strength in bending (*flexural strength* [12,13,18,22]) is little affected up to 200°C in lime-pozzolanic mortars with some white cement [13]. Portland-cement mortars have a similar behaviour (with/without small additions of graphite [18]), but their strength may even increase [12] up to 200°C. Blended cements (with either slag or pozzolane [12]) limit the strength loss to 20-40% up to 400-450°C. The flexural strength is, therefore, more heat-affected than the compressive strength, but less than the elastic modulus.

Like in concretes and masonry units, also in ordinary and high-performance mortars the stress-strain curves exhibit a linear + nonlinear + softening behaviour [14-16,21,24], but softening in heated mortars has been so far rarely investigated and measured [16,25].

Beside the maximum temperature (which is the major responsible for mortar damage [9,26,34]), other phenomena come into play, like thermal shocks (that depend on the heating and cooling rates) and the time length of the rest period at the maximum temperature. Compared with long rest periods (10h) and low heating rates (2°C/min), short rest periods (1h) and high heating rates (8°C/min) may increase the residual compressive strength, the flexural strength and the static modulus of elasticity by 40-60% at 600°C [18]. On the contrary, the greater thermal shock caused by cooling in water yields a greater strength reduction than cooling in air [27,28], especially if cement is partially replaced with silica fume (the residual flexural strength starts decreasing above 100°C rather than above 200°C [27]). As well, the time length past cooling and before testing plays a non-negligible role, as shown in [29], where re-curing in air after water/furnace/air cooling brings in a remarkable strength recovery in the first case (thanks to the transformation of calcium oxide into calcium carbonate), but does not prevent further strength losses in the other two cases. Concerning the heating rate, the few available specific studies show little and even contradictory effect on the residual properties of cement mortar [18,19].

Cementitious mortars exhibit also sizeable mostly unrecoverable thermal strains when heated for the first time (LITS = Load-Induced Thermal Strain [9,10,24,30,31]). These strains comprise the so-called transient creep, whose effect is to make strain and stress distributions in the mortar joints more uniform, to the benefit of masonry assemblies [32]. Research on heated concretes shows also that transient creep – which may occur without water exchange and independently from aggregates - is induced by microscopic changes in the hydrates, (particularly in the C-S-H hydrates [33]), leading to modifications of their properties.

Mortar structure has been investigated both at the micro- and meso-level [10,28,34], with specific attention to thermo-hygral phenomena [11,35,36], to the inclusion of polymeric, metallic, inorganic and hybrid fibres [37-39], to the replacement of cement with alkali-activated materials (*geopolymers* [40]), and to fracture energy [21,41]. In [38] polypropylene fibres are shown to be very effective in preventing thermal spalling in both autoclaved and water-cured high-strength mortars. All these cutting-edge issues are still open to investigation.

Within this complex context, one cement-lime mortar and two cement mortars are investigated in this project, to study their mechanical behaviour in ordinary conditions and after being exposed to high temperatures in quasi-steady thermal conditions (20, 200, 400 and 600°C). As well, the thermal diffusivity is evaluated (from 20 to 900°C [42]). In the first part of the paper, beside the thermal and mechanical properties as a function of the temperature, the evolution of the strengths on cubes and cylinders at high temperature is investigated and the stress-strain curves in compression are derived from the tests, with their extended softening branch. In the second part of the paper, a fairly simple analytical formulation is proposed for the stress-strain curves in compression, to incorporate temperature effect and mortar softening.

2. MATERIALS

Within an experimental campaign financially supported by a major Italian producer of construction materials (see the Acknowledgements), three bed-fixing cementitious mortars, indicated as “M5”, “M10” and “M15” in the following, were investigated. The three mortars belong to classes M5, M10 and M15 of the Italian standard [43], with $R_c \geq 5$, 10 or 15 MPa, respectively. Mortar M5 is considered as the *reference mortar*. Contrary to the higher-grade Mortars M10 and M15, M5 contains pp fibers ($v_f = 0.1\%$ by volume), but this very low fiber amount is assumed to have negligible effects on mortar performance compared with the performance of the other mortars. The main properties of the mortars – that are *pre-mixed* – are reported in Table 1. Lime was added to the mix as *slaked* (or *hydrated*) *lime*. The siliceous aggregates were introduced in saturated dry-surface conditions.

Table 1. Mix-design and main physical and mechanical properties of the mortars; the values (*, **) are the actual values: (*) 3.6% and (**) 2.9%.

Mix	**M5**	**M10**	**M15**
Lime [kg/m^3]	220	10	10
Cement [kg/m^3] – Portland R42.5	220	280	340
Siliceous aggregate (0-4 mm) [kg/m^3] (Italian Norm UNI EN 13139)	1220	1330	1380
Soluble chloride (Italian Norm UNI EN 1015-17)	≤ 0.05%		
Entrapped air (by concrete volume)	9.5%	2.5%	2.0%
Added water [kg/m^3] (w/c)	300 (1.36/1.07/0.88)		
Compressive strength on cylinders f_c [MPa]	5.1	8.4	12.1
Compressive strength on cubes R_c [MPa]	8.5	16.1	18.0
Nominal density ρ_N [kg/m^3]	1960	1920	2030
Actual density (after hardening) ρ [kg/m^3]	1758	1866	1982
Cement/lime/aggregate (by mass)	1/1/5.5	1/0*/4.8	1/0**/4.6
Cement+lime/aggregate (by mass)	0.36	0.22	0.22

The specimens to be tested in ordinary conditions and past cooling were supplied by the producer. To measure the thermal diffusivity between 20 and 900°C, special cylindrical moulds containing two thermocouples, their electrical cables and their fastening wires, were prepared by the authors and delivered to the producer of the mortars (see [44] for the technical details). The code provisions concerning each type of test are recalled in each sub-section.

3. EXPERIMENTAL PROGRAM

The compressive and tensile strengths, the elastic modulus, the density and the thermal diffusivity are among the main parameters to be evaluated in order to chacterize a mortar (as any other material), both in ordinary hygro-thermal conditions and at high temperature or after cooling down to room temperature.

In this project, twenty-four cylinders were cast to quantify the mass loss, to perform the tests in compression and to evaluate the elastic modulus (8 cylinders per each mortar; 2 for each of the 4 reference temperatures; diameter × height = 80 × 160 mm [43]). Three slightly larger and longer cylinders (∅ × h = 100 × 300 mm) were cast as well to evaluate the thermal diffusivity. Before casting, two thermocouples were properly fastened inside each cylinder by means of steel wires, with the electrical cables running longitudinally (i.e., parallel to the isotherm lines) [44]. One thermocouple was placed very close to the lateral surface and the other along the axis, both in the mid-height section of the specimen (Fig.2a).

In addition, 24 prisms (40 × 40 × 160 mm [43]) were cast for three-point bending tests aimed at measuring the indirect tensile strength. Following the bending tests, compression tests were carried out on the two stumps resulting from the fracture of each prism, with the load applied via two steel plates (40 × 40 mm [43]).

All cylinders were stored for 28 days inside plastic moulds, without plugs at the extremities, at 20-25°C and 60-70 R.H. After being removed from the moulds, the specimens

were cut to the desired length and the end sections were suitably ground, to achieve sufficient planarity and parallelism (∅/h = ½) [44,45].

All prisms were stored for 28 days in controlled thermo-hygral conditions (20°C, 95% R.H.) and this is the reason of their better performance in compression, compared with the cylinders, as discussed later [26].

Figure 2a shows a large cylinder inside the electric furnace before being heated to 900°C to evaluate the thermal diffusivity. The steel pipe around the specimen guarantees the homogeneity of the thermal field. The control parameter of the furnace is the temperature of the steel pipe. As for the small cylinders (to be tested past a thermal cycle), for each mortar and reference temperature two or three of them were heated at the same time in the furnace, without the steel pipe, since the control parameter was the internal temperature of the furnace as measured by the thermocopuple of the furnace. The tests in compression were performed not later than seven days past cooling. Each cylinder was provided with 3 LVDTs (base length = 50 mm) located at 120° in the mid-height section, to measure the shortening of the specimen. The same procedure was adopted for the prisms and cubes. The thermal cycles are sketched in Figure 2b.

In order to guarantee the uniformity of the thermal field and to avoid any self-stresses, the thermal cycles were performed in quasi-steady conditions (T_{max} = 200, 400 and 600°C). Each *heating and cooling cycle* consisted in a heating ramp at constant heating rate (1°C/min) up to the reference temperature T_{max}, a rest period at this temperature (120 minutes) and a cooling ramp at constant cooling rate (0.25°C/min) down to 200°C, followed by natural cooling inside the furnace, with the front door open. As usual in the high-temperature tests of cementitious materials, cooling was slower than heating to limit the extra damage induced in the material by the cooling phase, that is free of load-induced thermal strains [9,24].

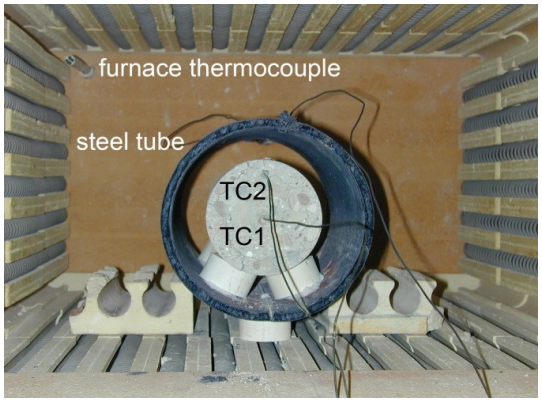

(a)

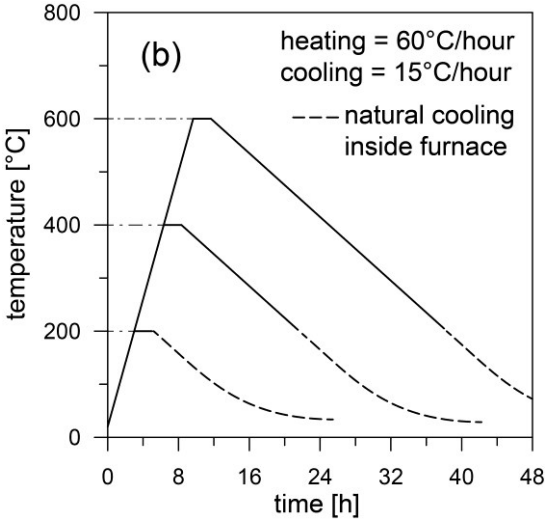

(b)

Figure 2. Electric furnace with a mortar cylinder instrumented with 2 thermocouples - TC1 and TC2 (a); and thermal cycles (b).

All the tests on the cylinders were displacement-controlled, with a displacement rate of 2.5 μm/s up to the maximum load, 5.0 μm/s in the softening branch down to 50% of the maximum load and 10.0 μm/s down to the crushing of the specimen. Note that the displacement rate 2.5 μm/s was derived from the provisions for testing concrete in compression (loading rate = 0.2-0.4 MPa/s [26]). As a matter of fact, in the tests on the lowest-grade mortar (M5, E_c = 8 GPa at 20°C, Fig.6b), the loading rate was exactly 0.4 MPa/s in the linear phase. The rate 2.5 μm/s was extended to all tests, for any mortar grade and

temperature.

Concerning the thermal cycles and the evaluation of the thermal diffusivity, there are no guidelines and code provisions. The authors have, therefore, adopted procedures and values used by most scholars (including the authors themselves) and well documented in the literature, for both concrete and mortars.

4. TEST RESULTS AND COMMENTS

The test results and – wherever necessary – details of the test procedures are presented and commented in the next sub-sections. As cement-based and cement-lime mortars are cementitious composites, reference is systematically made not only to the literature on mortars behaviour at high temperature, but also to the numerous results on concrete behaviour at high temperature.

4.1 Mass loss at high temperature

Prior to and after each thermal cycle, the weight of the specimen was measured to evaluate the mass loss per unit volume as a function of the temperature. The mass loss is roughly the same for the three mortars (Figure 3a) and is higher than in concrete (at 600°C, -12% compared with -5%, respectively [26]). The most probable reason is the higher water content of the mortars, where the water-cement ratio may exceed 90%, while the cement content is close to that of ordinary concrete. As an example, for a nominal mass at the fresh state of 1950 kg/m^3, cement content of 300 kg/m^3, added water equal to 300 kg/m^3 (cement/water ratio = 1), combined/bound water equal to 22% of the cement mass (66 kg) and free water in the capillary pores equal to 300 – 66 = 234 kg, the mass loss of the mortar at 600°C would be 234/1950 = 12% (practically coincident with the measured value), if the free water is assumed to be fully expelled at 600°C and the water contained in the aggregate is neglected.

Note that in the building site a sizeable quantity of the added water is lost in the passage from the fresh state to the hardened state, something that did not occur in the specimens cast in this project because they were cured in quasi-sealed conditions. Note also that the loss of the chemically bound water starts at 100-150°C, something that has not been considered in the previous calculations.

4.2 Thermal diffusivity

The thermal parameter controlling heat transmission by conduction is the thermal diffusivity D, that is the ratio between the heat transmitted and the heat stored by the unit mass of the material in question under a unit thermal gradient and in a unit time: $D = [L^2/t] = \lambda/(c\ \rho)$, where λ is the thermal conductivity, c is the specific heat and ρ is the mass per unit volume.

The thermal diffusivity can be easily determined at various temperatures by instrumenting *long cylinders* ($h \geq 2\varnothing$) subjected to a constant heating rate, fitted up with a couple of thermocouples placed at mid-height in the mid-section – one close to the external surface and the other along the axis ([42] Fig.2a).

In this research, three cylinders (one for each mortar, with $h = 2\varnothing$) were slowly heated from 20 to 900°C. As shown in Figure 3b, between 200 and 550°C the thermal diffusivity of the three mortars is roughly constant (= 0.25-0.35 mm^2/s) and by 30-35% lower than that of ordinary concrete, represented by the shaded envelope comprised between the two curves resulting from the upper and lower bounds indicated in Eurocode EC 2 [46] for the thermal conductivity. Hence, cementitious mortars effectively contribute to the insulation properties of masonry in firewalls.

Note that the change of state of the water from liquid to vapour in the capillary pores, and the change in the crystalline system (from α to β) of the quartz contained in the aggregates

are responsible for the downward spikes at 150-200°C and 550-580°C, respectively. (Both are endothermic phenomena) [9,10,12,26].

Below 100-150°C the *thermal transients*, and above 700-800°C *calcination* (= dissociation of calcium carbonate into calcium oxide and carbon dioxide) make the values of D doubtful.

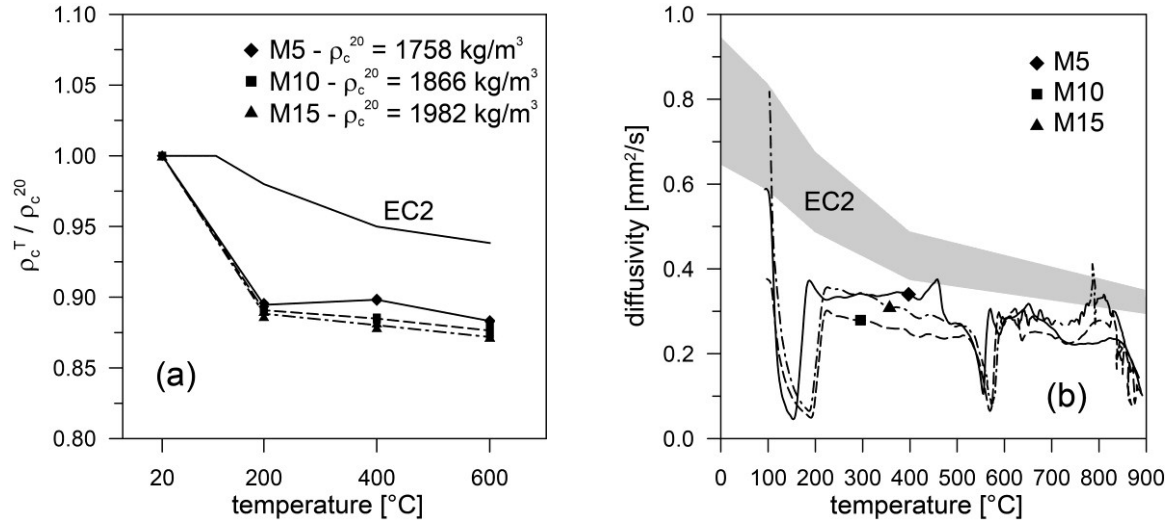

Figure 3. Diagrams of the density (a), and of the thermal diffusivity as a function of the temperature (b); the shaded envelope represents the thermal diffusivity of ordinary concrete according to EC2 [46].

4. 3 Stress-strain curves

Twenty-four cylinders (diameter × height = 80 × 160 mm) were tested in compression in displacement-controlled conditions, with the mortars either undamaged (T = 20°C) or past a thermal cycle (T = 200, 400 and 600°C). For each mortar and temperature, two tests were carried out, and in 80% of the tests the repeatability was satisfactory especially in terms of shape of the stress-strain curves.

As explained in Section 3, all cylinders were provided with 3 LVDTs (base length = 50 mm) located at 120° in the mid-height section, to measure the shortening of the specimen.

The fairly regular stress-strain curves (Figure 4) exhibit a noticeable ductility at 20, 400 and 600°C, but at 200°C the behavior becomes unexpectedly more brittle, in all mixes. The reason has probably to do with the expulsion and vaporization of the free water and with the beginning of the expulsion of the bound water, as testified by the downward peak in Figure 3b concerning the thermal diffusivity (150-200°C). In fact, past heating to 200°C, the residual mesostructure (weaker and more porous) may favor mortar brittleness, while at higher temperatures other phenomena prevail.

The strain at the peak stress is comprised between 1.2‰ and 2‰ at 20°C (as in concrete), decreases at 200°C (close to 1‰), and finally starts increasing at higher temperatures (2-3‰ at 400°C and 4-5‰ at 600°C). The strength loss between 20 and 600°C is comprised between 61% (M5) and 66% (M15). Limited comparisons can be made with the well-documented *hot tests* presented in [16] on a high-performance cementitious mortar, where the strain at the stress peak is comprised between 2 and 6‰ (for T = 20 and 500°C, respectively), with a strength loss close to 64% at 500°C. Mortars similar to those investigated in this paper (called in the same way "M5" and "M10") were tested at high temperature in [14, 15] (*hot tests* up to 600°C), but in this case the strains at the stress peak were definitely larger (from 4 to 12‰ and from 6 to 13‰ in M10 and M5, respectively, for T = 20-600°C) and the strength loss

definitely lower (24 and 31% at 600°C) compared with authors' *residual* tests. In [14, 15] no information is given on mortar softening in compression, since the tests were stopped at the stress peak. Note that similar differences on the strains, between *hot* and *residual* tests at high temperature, were found in [25] concerning a very high-strength microconcrete.

In Figure 4, each curve is the average of two experimental curves, except at 200°C, where a few experimental curves were not complete, because of press or specimen malfunctioning.

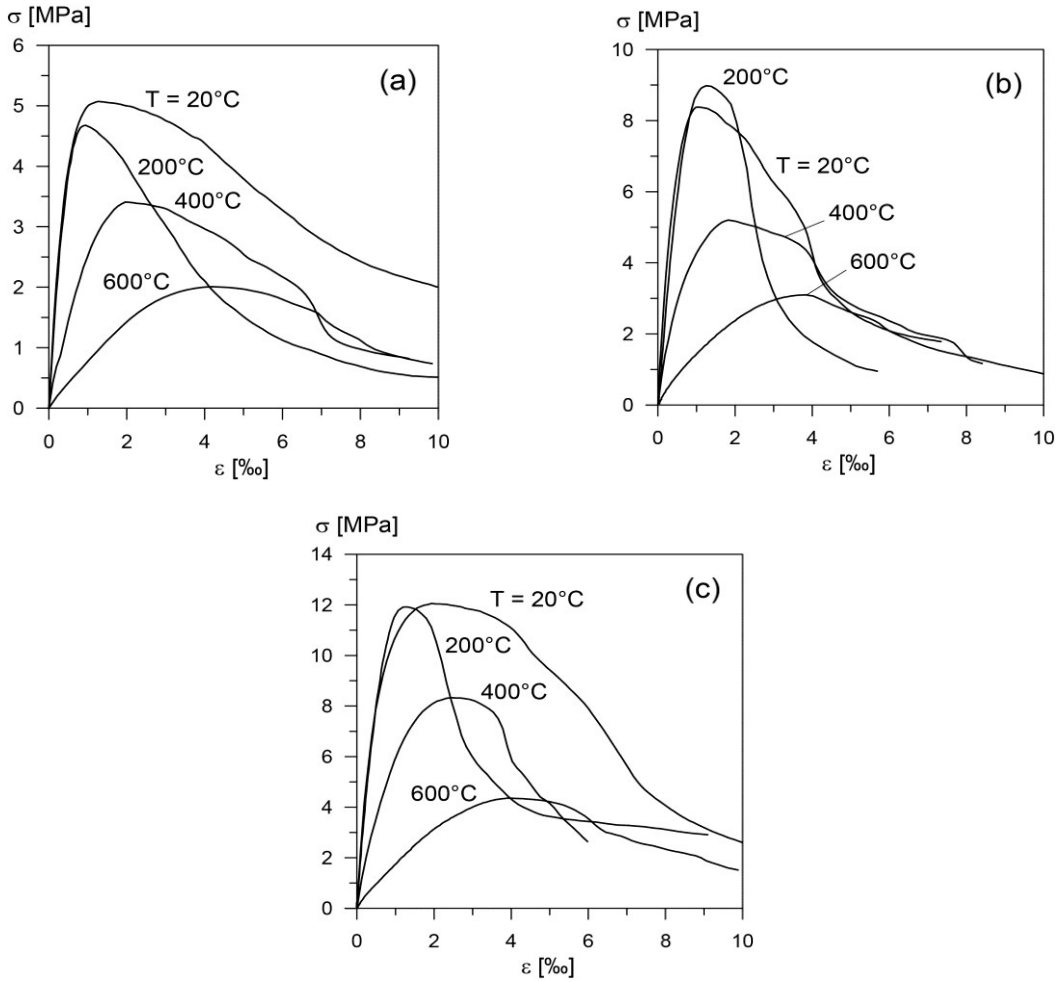

Figure 4. Average stress-strain curves for Mortars M5 (a), M10 (b) and M15 (c).

Though rather low, the values of the cylindrical strength at 20°C (f_c = 5.1, 8.2 and 12.0 MPa; mean values of two tests) agree with producer's indications (R_c = 8, 14 and 17 MPa) and with the tests on small cubes (R_c = 8.5, 16.1 and 18.0 MPa, Figure 8a), provided that the following factors are taken into account: (a) the larger – and favourable – effect of friction in the small specimens tested by the producer for material certification (cubes with side = 40 mm); (b) the brittleness of the material and the ensuing *size effect*, more favourable in small than in large specimens [47]; and (c) curing inside a plastic mould (as done in this study) rather than in a controlled environment [26] (for further details see [44]).

Hence, it is reasonable that f_c measured on medium-size cylinders (∅, h = 80, 160 mm) be close to 60-70% of R_c measured on small cubes. (The commonly-found value of the ratio f_c/R_c falls in the range 0.80-0.85 [26], when ordinary cylinders and cubes are tested; in the authors' experience, 0.83 is the value closest to test results).

On the whole, the higher the mortar grade, the higher the negative slope of the softening branch, this being an indication of the decreasing toughness with mortar strength. In all cases,

the initial stiffness (or modulus of elasticity at the origin) is deeply affected by the temperature.

4.4 Mechanical and kinematical properties

4.4.1 Compressive strength

Mortar M15 exhibits the best performance at any temperature (Figure 5a: at 600°C the residual strength of Mortar M15 is twice as much that of the *reference* Mortar M5). In terms of *normalized* compressive strength (Figure 5b), M10 and M15 behave somewhat better than M5 up to 300°C, while there are no practical differences above 400°C. The normalized curves, however, are very close and may be represented by means of a single second-order parabola, as will be shown later.

In Figure 5b, the results of this study confirm those available in the literature (shaded envelope comprising hot and residual tests, tests on cubes and on cylinders). The increase in strength up to 250-300°C, exhibited by a number of tests, often occurs also in concrete, but – as in concrete – it is of no practical relevance. Note that the envelope in Figure 5b is based on the tests presented in [12,17,18,20,27]. Note also that in [18] the focus is on high-performance mortars, and that the tests after air cooling presented in [27] are not introduced in Figure 5b, because their results tend to be off-scale.

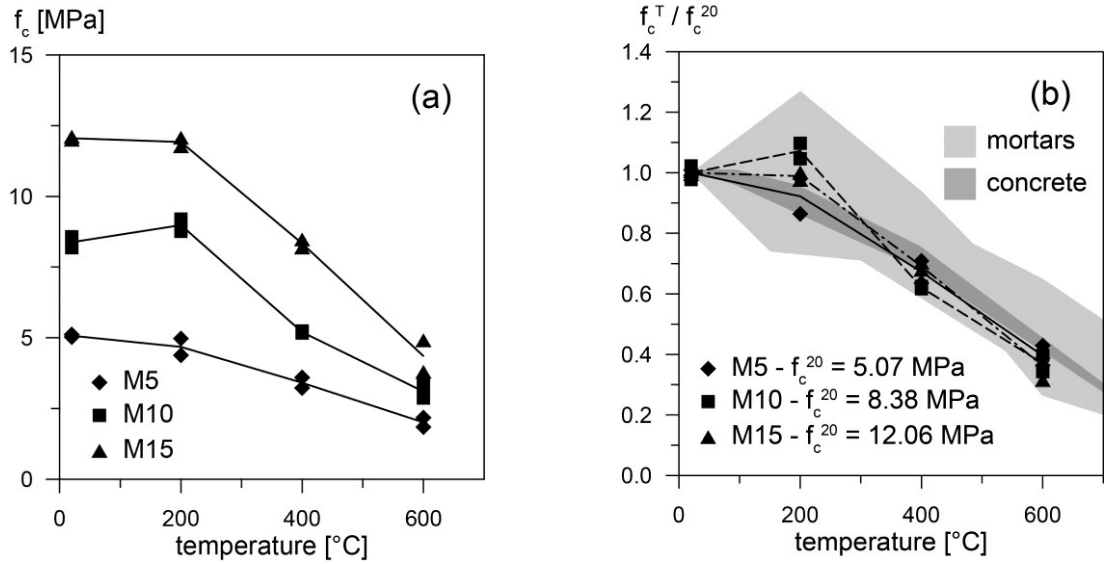

Figure 5. (a) Diagrams of the compressive strength on cylinders; and (b) normalized diagrams.

Finally, the strength decay similar to that of ordinary concrete (EuroCode EC2, Structural Fire Design [46], dark-gray area) is a clear indication that in any walls made of concrete blocks mortar layers are not the *weakest link of the resisting chain*, at any temperature, all the more because mortar layers generally are in *confined conditions*, which are always favorable to the mechanical performance of cementitious materials.

4.4.2 Elastic modulus

The secant modulus was evaluated from the stress-strain curves, in the stress range 30-50% with respect to the peak of the stress-strain curves (Figure 6a).

The values at 20°C are very low compared with those of ordinary concrete, something well known for mortars. In fact, using for mortars the highly-reliable relationship given in EC2 [48] for concrete ($E_c = 22000 \cdot [f_c/10]^{0.3}$, where E_c and f_c are in MPa), the values of the elastic

modulus of the mortars would be comprised between 44% (M5) and 60% (M15) of those of ordinary same-strength concretes.

The normalized performance of Mortar M15 is the best up to 400°C; above this temperature, there are no practical differences between M15 and M10. The normalized values (Figure 6b) are in good agreement with the cloud resulting from the tests presented in [18, 39] and confirm – also for cement-lime mortars and cement-based mortars that the heat-triggered decay of the elastic modulus is larger than that of the compressive strength (compare Figure 6 with Figure 5).

As in the case of the compressive strength, the normalized curves of the secant elastic modulus are rather close (Figure 6b) and a single second-order parabola may be adopted for the three mortars, as will be shown later.

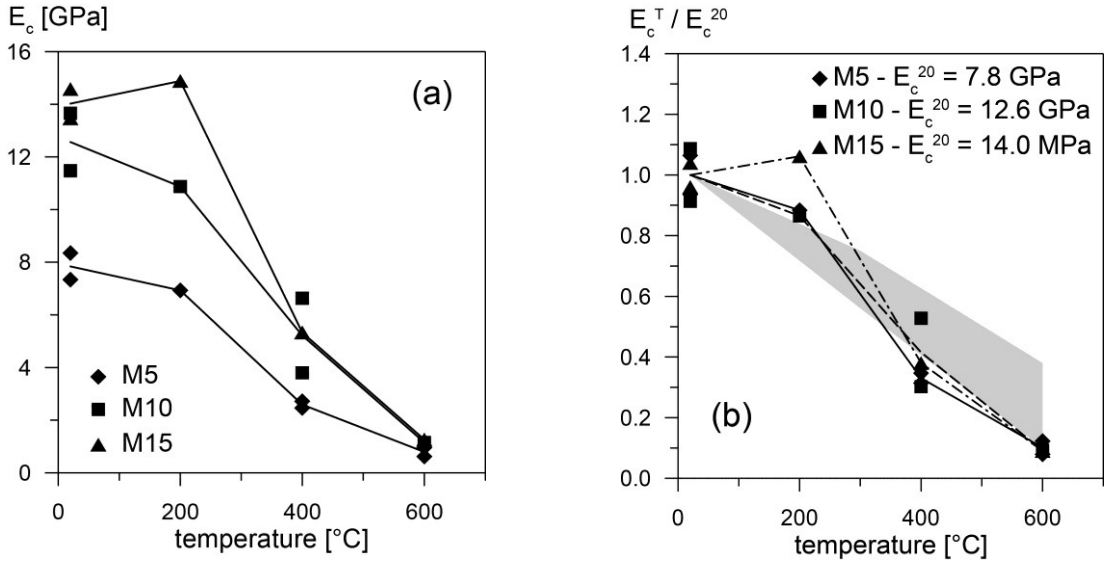

Figure 6. (a) Diagrams of the elastic secant modulus; and (b) normalized diagrams.

4.4.3 Tensile strength in bending

As previously mentioned, the indirect tensile strength was evaluated by loading to collapse prismatic specimens (size 40×40×160 mm) subjected to 3-point bending, according to a well-known procedure [43]. The remaining stumps were later tested in compression, by applying the load through two 40×40 mm steel plates, in order to measure the strength on cubes (R_c).

The stronger mortars (M10 and M15) behave in the same way (Figure 7a) and better – as should have been expected - than the lowest-grade mortar (M5). The normalized curves (Figure 7b), however, are very close and confirm the linear decrease of the tensile strength with the temperature, which is well known in ordinary concrete.

The values of the tensile strength in bending are close to – or included inside – the cloud of the tests presented in [12, 18, 27, 39]. As in the case of the compressive strength, the tests in [18] refer to high-performance mortars, and the tests after water cooling presented in [26] are not included in the cloud of Figure 7b, because their results tend to be off-scale.

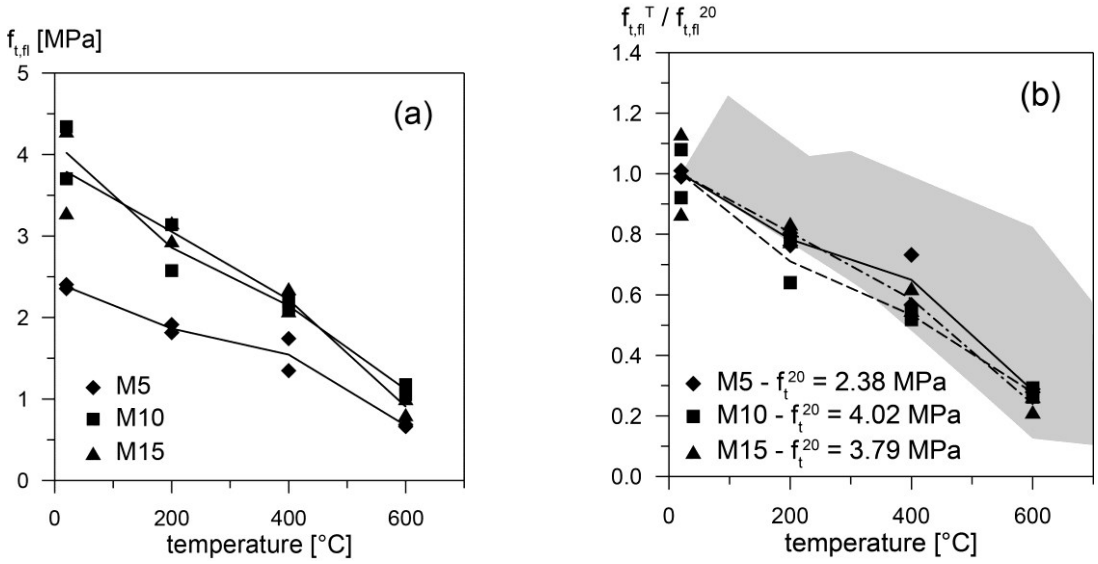

Figure 7. Indirect tensile strength in bending: (a) diagrams in 3-Point bending (prism size a × b × L = 40 × 40 × 160 mm^3); and (b) normalized diagrams.

4.4.4 Strain at the stress peak

The strain at the stress peak (*peak strain*) resulting from the stress-strain curves (Figure 4) is plotted in Figure 8 for the three mortars investigated in this study. On the whole, at any temperature the values are rather close and exhibit a definite upward trend with the temperature, except below 200°C, where the trend is mixed, with contradictory results, as Mortars M5 and M15 exhibit a reduction in terms of peak strain and M10 a slight increase. Equation 4 (proposed in Section 6) provides an approximate description of strain evolution up to 600°C.

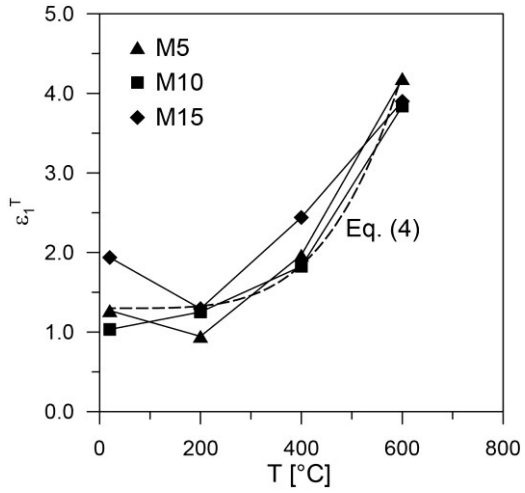

Figure 8. Strain ε_1 as a function of the temperature, and plot of $\varepsilon_1^T/\varepsilon_1^{20}$ (Eq.4).

5. STRENGTH ON CUBES VS. STRENGTH ON CYLINDERS

The residual cube strength exhibits a fairly linear decrease with the temperature as shown by the normalized curves R_c^T/R_c^{20} (Figure 9a), which are very close and can be represented by means of a single straight line (dash line, Figure 9b). Note that the standard curing applied to the prisms after casting makes the strength on cubes very close to – or even higher than - the

expected values (R_c = 18, 16 and 8.50 MPa at 20°C).

In Figure 9b the normalized strength on cylinders (f_c^T/f_c^{20}) is plotted as well (dash-dotted curve, mean curve resulting from the diagrams in Figure 6b). Since virtually all the tests on mortars are carried out on (small) cubes and often the tests on cementitious composites exposed to high temperature are performed on either cubes or cylinders, quantifying the effect of the temperature on the ratio f_c^T/R_c^T is quite interesting, all the more because experimental results on concrete are scanty indeed [49] and on mortars are nonexistent.

The passage from R_c^T/R_c^{20} and f_c^T/f_c^{20} to f_c^T/R_c^T involves the ratio f_c^{20}/R_c^{20}:

$$f_c^T/R_c^T = (f_c^T/f_c^{20}) \times f_c^{20}/[(R_c^T/R_c^{20})\times R_c^{20}] = [(f_c^T/f_c^{20})/(R_c^T/R_c^{20})] \times (f_c^{20}/R_c^{20}) \quad (1)$$

The value of the ratio (f_c^{20}/R_c^{20}) is close to 0.60 in this project (tests on small cubes vs. tests on medium-size cylinders; cubes and cylinders cured in different conditions, see Section 4.3). For similar dimensions and curing conditions, the generally found value in the literature is 0.80-0.85 (often-accepted value = 0.83). Hence, to make the tests on cylinders comparable with those on cubes, the ratio (f_c^{20}/R_c^{20}) should be multiplied by 0.83/0.60 = 1.38, as done in Figure 9b (thick full curve).

Figure 9b clearly indicates a tendency for the ratio f_c^T/R_c^T to decrease with the temperature (above 200°C). Such a fact should always be kept in mind whenever the results coming from different experimental campaigns on cementitious materials are compared. For instance, after heating to 600/800°C a mortar specimen and cooling down to room temperature, the ratio f_c^T/R_c^T is close to 0.75/0.55 instead of 0.80-0.85.

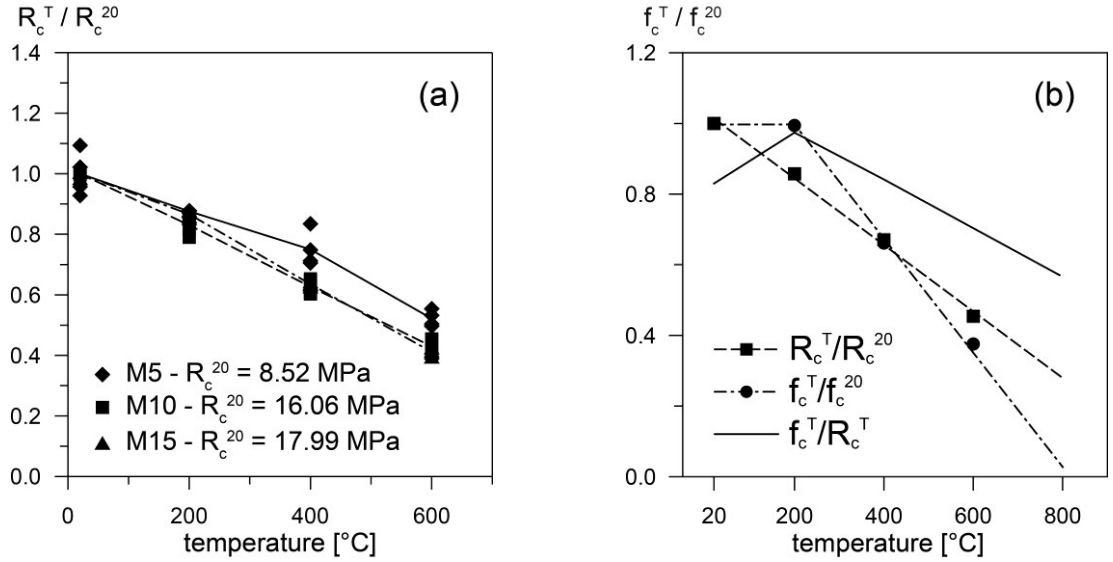

Figure 9. Normalized diagrams of the compressive strength on cubes (a); and normalized diagrams of the strengths on cubes and cylinders, and of their ratio as a function of the temperature (b).

6. ANALYTICAL EXPRESSION FOR THE STRESS-STRAIN LAW IN COMPRESSION

The stress-strain curves shown in Figure 4 give plenty of information about certain typical points (like P_0, P_1 and P_2 in Figure 10a) whose properties are instrumental in working out an appropriate analytical formulation for the stress-strain curve in compression or to calibrate already available formulations. To this aim, as a first step such parameters as the compressive

strength (peak stress) $\sigma_1 = f_c$ and its strain ε_1, the tangent elastic modulus at the origin E_0, the stress σ_2 and the strain ε_2 at the contraflexure point of the softening branch should be expressed as a function of the temperature (σ_2 - which is close to $4/5 f_c$ at any temperature – and ε_2 will not be considered in the following).

Figures 5b and 6b allow expressing the normalized compressive strength and elastic modulus as a function of the temperature, through the following simple relationships (Figure 10b):

$$f_c^T/f_c^{20} = 1 - 1.75\,[(T - 20)/1000]^2 \quad (2)$$

$$E_c^T/E_c^{20} = 1 - 2.63\,[(T - 20)/1000]^2 \quad (3)$$

Note that f_c^{20} in Eq.2 is either indicated by the structural designer or inferred from in-situ tests, while E_c^{20} in Eq.3 may be derived from the equations used for concrete, provided that a reduction factor be introduced to take care of the lesser stiffness of mortar compared to concrete. (In Section 4.3, the value of this reduction factor is shown not to exceed 0.6; hence, 0.60 may be a reasonable guess: $E_c^{20} = 0.6 \times 22000 \cdot [f_c/10]^{0.3}$).

As for the strain ε_1 at the stress peak (Point P_1), the values plotted in Figure 8 indicate that ε_1 as a function of the temperature may be roughly represented by means of a single curve, whose analytical expression is provided by Eq.4 (Figure 8 dash curve and Figure 10b):

$$\varepsilon_1^T/\varepsilon_1^{20} = 1.0 + 20\,[(T - 20)/1000)]^4 \quad \text{where} \quad \varepsilon_1^{20} = 1.30‰ \quad (4)$$

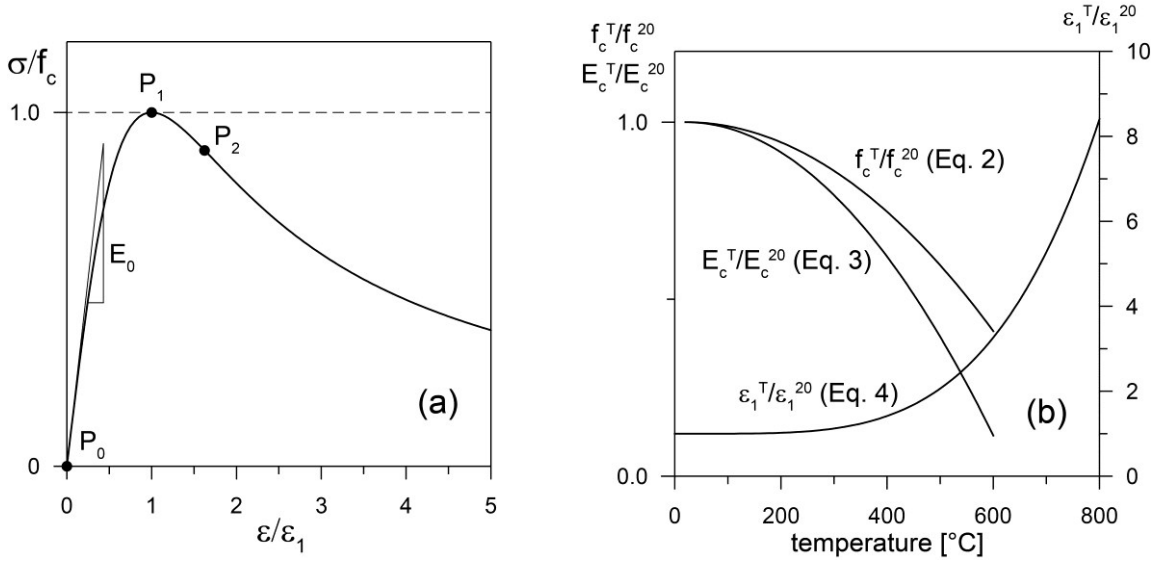

Figure 10. Qualitative stress-strain curve with the reference points P_0, P_1 and P_2 (a); and plots of f_c^T/f_c^{20} - Eq. 2, E_c^T/E_c^{20} - Eq. 3, and $\varepsilon_1^T/\varepsilon_1^{20}$ - Eq.4 (b).

As for the analytical formulation of the normalized stress-strain curve, the functional dependency provided by EC2 [46] for concrete is adopted (Eq.5), but with two open issues concerning the value of the parameter n, that controls the general shape of the curve and specifically the steepness of the softening branch:

$$\underline{\sigma} = n \cdot \underline{\varepsilon}/[(n - 1) + \underline{\varepsilon}^n] \quad (5)$$

where $\underline{\sigma} = \sigma/f_c$, $\underline{\varepsilon} = \varepsilon/\varepsilon_1$ and $n > 1$.

The open issues are:

- Should n be constant and independent of the temperature as proposed in EC2 for concrete, or should it be variable as a function of the temperature?
- Should the value(s) of n be close to that of concrete (n = 3) or should the value(s) be smaller to take care of the greater ductility of the mortars?

Note that the larger the values of n, the sharper the stress peak ($\sigma = f_c$) and the steeper the softening branch. Large values of n represent, therefore, brittle materials.

Finding a possible dependency of n on T is the objective – and the original contribution – of this section.

Equation 5 complies with the following four conditions:

- $\sigma = 0$ for $\varepsilon = 0$;
- $\sigma = f_c$ for $\varepsilon = \varepsilon_1$;
- $\sigma = \sigma_{max}$ for $\varepsilon = \varepsilon_1$;
- $\sigma \rightarrow 0$ for $\varepsilon \rightarrow \infty$

To determine n, one further condition should be enforced; there are at least three alternate approaches:

- $[d\sigma/d\varepsilon]_{\varepsilon=0} = E_{c0}$ where E_{c0} = tangential elastic modulus; enforcing this condition is mandatory if the objective is a correct description of the loading (mostly linear) branch;
- $\sigma = \sigma_2$ for $\varepsilon = \varepsilon_2$ if the objective is a fairly realistic – albeit simplified - description of the softening branch (counterflexure, however, is not enforced); in a few numerical tests performed by the authors this approach did not lead to acceptable results in terms of stress-strain curves and – as previously said – this approach was abandoned;
- adopting a *best-fit* procedure to describe in the best possible way the trend indicated by the test results, with or without the passage through the point of the maximum stress where $\sigma = \sigma_1 = f_c^T$ and $\varepsilon = \varepsilon_1^T$.

Note that $E_{c0} = 1.1\text{-}1.2\ E_c$ with E_c = secant modulus. (In the following: $E_{c0} = 1.15E_c$).

By adopting the first of the three above-mentioned alternate approaches, the following results are obtained:

$$n = E_{c0}/[E_{c0} - (f_c/\varepsilon_1)] \quad (n^* \text{ in Figure 11a}) \tag{6a}$$

$$\underline{\varepsilon_2} = (n + 1)^{1/n} \quad \text{and} \quad \underline{\sigma_2} = (1/2) \cdot (n + 1)^{1/n} \tag{6b,c}$$

Since the expressions of E_{c0}^T, f_c^T and ε_1^T as a function of T are known, the variables n^T, ε_2^T and σ_2^T can be calculated.

For mortars M5, M10 and M15, the values of the parameter n and their trend curves are plotted in Figure 11a (first approach) and Figure 11b (third approach).

In both cases the values of n look fairly low (compared with n = 3 proposed for concrete), but – in spite of the sizeable dispersion - the parameter n exhibits a slight increase with the temperature up to 400°C and a fast increase above 400°C, as indicated by the *average curves* in Figures 11a and 11 b (*dash curves*). The normalized values $n^T/n^{20} = n(T)/n^{20}$ (Figure 11c, see absolute values in Figure 11b) can be fitted with a single curve (dash curve, Eq.7, Figure 11c):

$$n^T/n^{20} = 1 + a\,(T - T_0)/T^* + b\,[(T - T_0)/T^*]^4 \tag{7}$$

where: a = 0.5 ; b = 5.4 ; T_0 = 20°C ; T* = 1000°C.

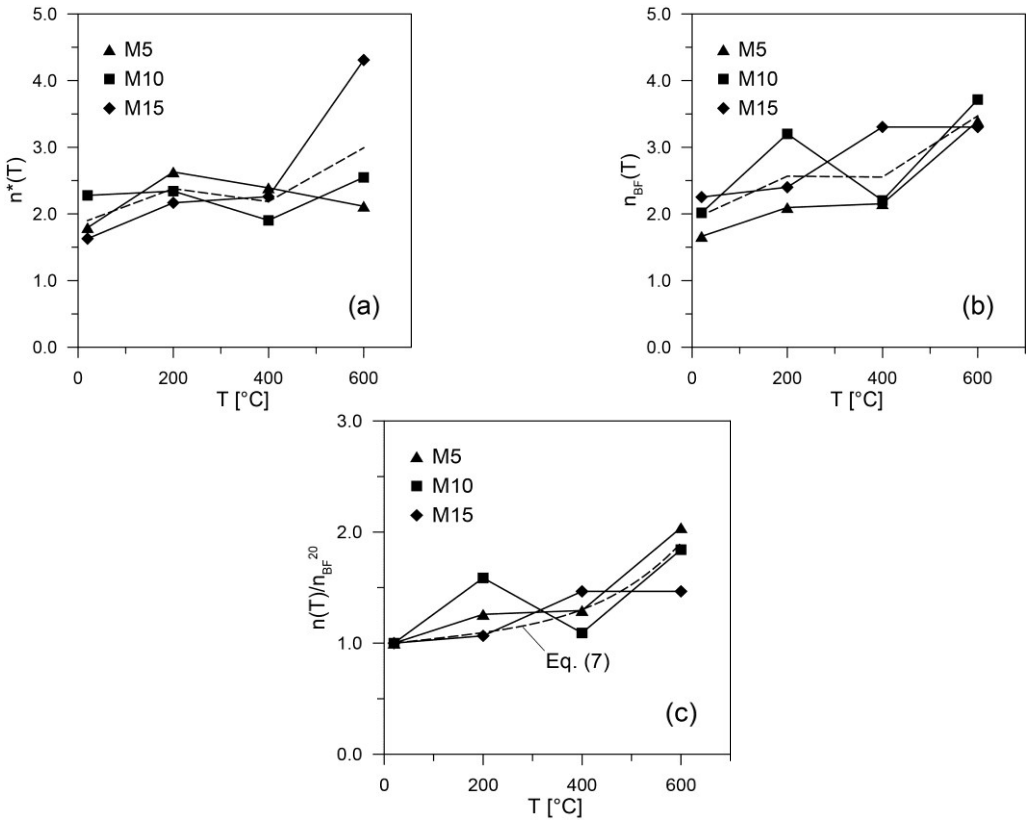

Figure 11. Plots of n as a function of the temperature: n* according to the first approach (a); and n_{BF} according to the third approach – *best-fit* approach (b); and normalized values (c) based on the third approach, where n_{BF}^{20} = 1.6, 2.0 and 2.3 for M5, M10 and M15, respectively. The dash curves in (a) and (b) represent the average trends.

The stress-strain curves are plotted in Figures 12, 13 and 14 for mortars M5, M10 and M15, respectively, for n variable with T according to the best-fit procedure (full curves in Figure 11b) and to Eq.7 (dash curve in Figure 7c). The experimental curves are plotted as well for T = 20 and 400°C (Figs.12a, 13a, 14a), and for T = 200 and 600°C (Figs.12b, 13b, 14b).

As expected, n as a function of T (Eq.7) is less effective in describing the softening behavior of the mortars than n resulting from the best-fit procedure, but the differences tend to vanish for T ≥ 400°C. The value n = 3 proposed in EC 2 for the loading branch of concrete stress-strain curve – and often extended to the entire response curve, softening included - would not be appropriate for the full stress-strain curves of the mortars, because such a high value as n = 3 would overrate the brittleness of the mortars (with a very steep softening branch not exhibited by the mortars investigated in this study).

Looking at Figures 12-14, one may observe that the analytical expressions derived from the tests about the normalized compressive strength, elastic modulus and strain at the stress peak (Eqs.2-4) - together with the parameter n calibrated on the former three normalized parameters (Eq.7) – make it possible to describe more than satisfactorily (through Eq.5) the uniaxial behavior in compression of the lime-cement and cement mortars investigated in this research project.

The general approach presented in this section may also be applied to other mortars and cementitious materials, based on a fairly limited number of tests.

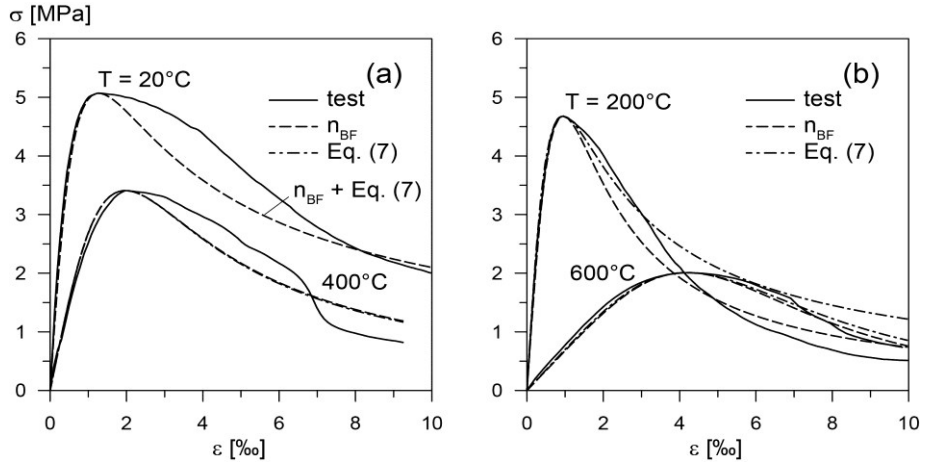

Figure 12. Stress-strain curves of mortar M5: (a) T = 20 and 400°C; and (b) T = 200 and 600°C, for n = n(T) from Eq.7, and n = n_{BF} (best-fit, full curve in Figure 11b);
the full curves stand for the tests.

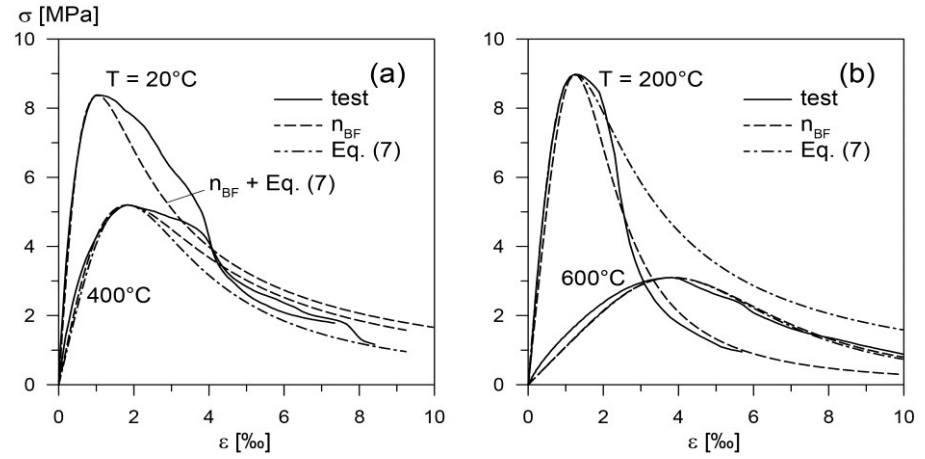

Figure 13. Stress-strain curves of mortar M10: (a) T = 20 and 400°C; and (b) T = 200 and 600°C, for n = n(T) from Eq.7, and n = n_{BF} (best-fit, full curve in Figure 11b);
the full curves stand for the tests.

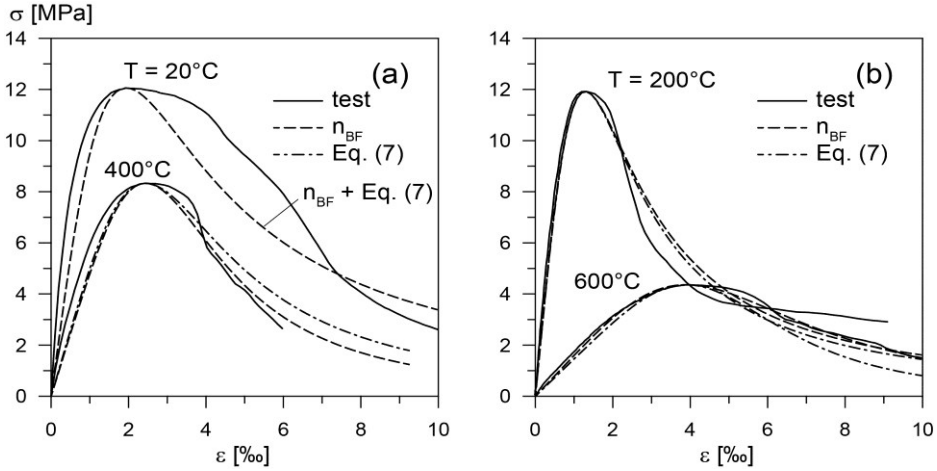

Figure 14. Stress-strain curves of mortar M15: (a) T = 20 and 400°C; and (b) T = 200 and 600°C, for n = n(T) from Eq.7, and n = n_{BF} (best-fit, full curve in Figure 11b);
the full curves stand for the tests.

7. CONCLUSIONS

The residual tests carried out on three mortars (lime-cement mortar M5, and cement mortars M10 and M15, with a strength on cubes in excess of 5, 10 and 15 MPa) show that even after a thermal cycle at high temperature ($T \leq 600°C$ for the mechanical properties and mass loss, and 900°C for the thermal diffusivity) these mortars still retain significant capacity; in detail:

- the three mortars keep very good insulation properties at any temperature up to 900°C, as demonstrated by their thermal diffusivity, which is definitely lower than that of ordinary concrete at any temperature;
- as expected, the mass loss per unit volume is greater than that of ordinary concrete, because of the larger amount of water in the mix design of the mortars;
- the two higher-grade mortars (M10 and M15) are slightly less heat sensitive in compression than the reference mortar (M5) below 300°C; above this temperature, the normalized diagrams tend to coincide; on the whole, the mechanical decay agrees with the cloud of the test results available in the literature on mortars and is very close to the mechanical decay of concrete;
- in terms of secant elastic modulus, the highest-grade mortar is more heat-sensitive than the other two mixes, but above 400°C there are no differences between the two highest-grade mortars; the normalized curves, however, are very close and are also close to the lower bound of the tests on mortars documented in the literature;
- in terms of residual strength in indirect tension in bending (*flexural strength*), there is a coincidence between the absolute values pertaining to the two highest-grade mortars, which behave better than the lowest-grade mortar, but the normalized diagrams are very close, and the decay with the temperature is roughly linear; on the whole, the normalized curves are close to the lower bound of the tests on mortars documented in the literature;
- in terms of compressive strength, testing cubes is not only questionable at room temperature, but may even be erroneous at high temperature and after cooling, because of the different effect of temperature on the strength on cubes with respect to that on cylinders (the greater role of cube-to-press friction in the former case introduces a favorable confining effect, that increases with the temperature and the decay of the material);
- the residual stress-strain curves in compression are similar to those of other cementitious materials, with an initial linear behavior, a loss of linearity, a more or less sharp peak and a rather steep softening branch; the behavior of the three cementitious mortars investigated in this project, however, looks more ductile than that of concrete at any temperature except at 200°C, where the three mortars exhibit a rather brittle behavior, to be further investigated; compared with some data in the literature, cementitious mortars look less ductile than lime mortars, at any temperature;
- the analytical formulation proposed in EC 2 for the stress-strain curve of concrete – based on the ratio between a linear function of the strain and a higher-degree polynomial – may still be adopted in mortars, on condition that the parameter controlling the general shape of the curve be given values slightly increasing with the temperature and smaller than the constant value proposed for concrete;
- in general, the proposed formulation for the stress-strain curve realistically predicts the behavior of cementitious mortars at and above 400°C, but tends to underrate the ductility at 20°C and the steepness of the softening branch at 200°C, that is well described only in the highest-grade mortar.

The tests presented and discussed in this paper show that (a) the mechanical decay of traditional cementitious mortars exposed to high temperatures is similar to that of concrete, both in uniaxial tension and compression, and (b) the insulation properties – represented by the thermal diffusivity - are little affected by the temperature. Hence, mortars are not the *weakest ring of the resisting chain* in brick and block walls exposed to the fire, all the more because the friction between the mortar layers and the bricks or blocks tends to create a favorable well-known 3D state of stress in the mortar layers, through a *confining action*.

ACKNOWLEDGEMENTS

This project was financially supported by the firm VAGA (of MAPEI Group, Treviso, Italy); the authors are indebted to MS Engineers Emanuele Della Pasqua and Enrico Parmini for their valuable assistance.

REFERENCES

[1] Sciarretta, F., Antonelli, F., Peron, F., Caniglia, S. (2018) Final outcomes on the multi-disciplinary long-term monitoring and preservation-state investigation on the medieval external Façades of Palazzo Ducale in Venice, Italy, Journal of Civil Structural Health Monitoring 8(1), pp. 111-133

[2] EN 998-2 (2016) Specification for mortar for masonry - Part 2: Masonry mortar, European Committee for Standardization, Brussels, Belgium.

[3] Shoaib, M. M., Ahmed, S. A., Balaha, M. M. (2001) Effect of fire and cooling mode on the properties of slag mortars, Cement and Concrete Research, 31, pp. 1533-1538

[4] Mortar Industry Association (2013) Introduction to Modern Mortars, Learning Text part 01, Mineral Products Association Ltd, London, UK

[5] Moghadam, M. A., Ramezan, A. I. (2020) Effects of zeolite and silica fume substitution on the microstructure and mechanical properties of mortar at high temperatures, Construction and Buildimg Materials, 253, 119206

[6] Eurocode 6 – EN 1996-1-2 (2007) Design of Masonry Structures, Part 1-2: General Rules – Structural Fire Design, European Committee for Standardization, Brussels, Belgium

[7] Gambarova, PG, Fantilli, A, Tattoni, S (Editors, 2017) Fire-Resistant Structures (in Italian), EPC (Roma, Italy), 501 pp.

[8] Tate, M. (2005) The Most Important Property of Cement-Lime Mortar in Masonry Construction is…, Proc. Int. Building Lime Symposium 2005, Orlando (Florida, USA), March 9-11, 13 pp.

[9] Khoury, A.G. (2000) Effect of Fire on Concrete Structures, Progress in Structural Engineering Materials, 2, pp. 429-447

[10] Castellote, M, Alonso, C, Andrade, C, Tirillas, X, Campo, J (2004) Composition and Microstructural Changes of Cement Pastes upon Heating as Studied by Neutron Diffraction, Cement and Concrete Research, 34(9), pp. 1633-1644

[11] Černý, R, Maděra, J, Poděbraská, J et al. (2000) The effect of compressive stress on thermal and hygric properties of Portland cement mortar in wide temperature and moisture ranges, Cement and Concrete Research, 30(8), pp. 1267-1276

[12] Andiç-Çakir, Ö, Çopuroğlu, O, Ramyar, K (2008) Effect of High Temperature on Mechanical and Microstructural Properties of Cement Mortar, 11th Int. Conf. on Durability of Building Materials and Components - 11DBMC, Istanbul (Turkey), May 11-14, Paper T11, 7 pp.

[13] Pachta, V, Triantafyllaki, S, Stefanidou, M (2018) Performance of lime-based mortars at elevated temperatures, Construction and Building Materials, 189 (11), pp. 576-684

[14] Andreini, M, De Falco, A, Sassu, M (2014), Stress-strain curves for masonry materials exposed to fire action, Fire Safety Journal, 69, pp. 43-56

[15] Andreini M., Caciolai M., La Mendola S., Mazziotti L., Sassu M. (2014) Mechanical behavior of masonry materials at high temperature, Fire and Materials, DOI: 10.1002/fam.2229

[16] Fu, YF, Wong, YL, Poon, CS et al. (2004) Experimental study of micro/macro crack development and stress-strain relations of cement-based composite materials at elevated temperatures, Cement and Concrete Research, 34(6), pp. 789-797

[17] Yazici, Ş, Sezer, GÎ, Şengül, H (2012) The effect of high temperature on the compressive strength of mortars, Construction and Building Materials, 35(10), pp. 97-100

[18] Cülfik, MS, Özturan T (2002) Effect of elevated temperatures on the residual mechanical properties of high-performance mortar, Cement and Concrete Research, 32(5), pp. 809-816

[19] Hossain, MA, Islam, MN, Karim, MR (2006) Fire Resistance of Cement Mortar Containing High-Volume Fly Ash, Proc. 31st Conf. on Our World in Concrete & Structures, Singapore, August 16-17, 5 pp.

[20] Morsy, MS, Rashad, AM, Shebl, SS (2008) Effect of elevated temperature on compressive strength of blended cement mortar, Building Research Journal, 56(2-3), pp. 173-185

[21] Bamonte, P, Gambarova, PG (2014) Properties of Concrete Subjected to Extreme Thermal Conditions, Journal of Structural Fire Engineering, 5(1), pp. 47-62

[22] Sciarretta, F. (2014) Modeling of mechanical damage in traditional brickwork walls after fire exposure, Advanced Materials Research - Trans Tech Publications Ltd, 919, pp. 495-499

[23] Russo, S., Sciarretta, F. (2015) Numerical investigation on the residual behaviour of masonry walls damaged by fire exposure, Key Engineering Materials, 624, pp. 230-237

[24] Dias, WPS, Khoury, GA, Sullivan, PJE (1990) Mechanical Properties of Hardened Cement Paste Exposed to Temperatures up to 700°C (1292°F), ACI Materials Journal, 87(2), pp. 160-166

[25] Bamonte, P., Gambarova, P.G. (2010) Thermal and mechanical properties of a very high-strength durable concrete, ASCE-Journal of Materials in Civil Engineering, 22 (6), pp. 545-555

[26] Neville, AM (2011) Properties of Concrete, 5th Edition, Pearson Education Limited, 846 pp.

[27] Yüzer, N, Aköz, F, Öztürk, LD (2004) Compressive strength-color change relation in mortars at high temperature, Cement and Concrete Research, 34(10), pp. 1803-1807

[28] Messaoudene, I, Molez, L, Jauberthie, R, Kessal, O, Slama, L (2015) Effect of the Quenching in Water of the Cementitious Materials Subjected to Fire, Université Mohamed Khider (Algérie), publ. in Courier du Savoir, 20, December 2015, pp. 9-14

[29] Karahan O. (2010) Residual compressive strength of fire-damaged mortar after post-fire air curing, Fire and Materials, pub. on line 16 November 2011, DOI.org/10.1002/fam.1074

[30] Thienel, K-Ch, Rostásy, FS (1996) Transient creep of concrete under biaxial stress and high temperature, Cement and Concrete Research, 26(9), pp. 1409-1422

[31] Torelli, G, Mandal, P, Gillie, M, Tran, VX (2016) Concrete strains under transient thermal conditions: a state-of-the-art review, Engineering Structures, 127, pp. 172-188

[32] Ravi Prakash, P., Azenha, M., Pereira, J. M., Lourenço, P. B. (2020) Finite element based micro modelling of masonry walls subjected to fire exposure: framework validation and structural implications, Engineering Structures 213, 110545

[33] Cagnon, H., Vidal, T., Sellier, A., Camps, G. (2014) Influence of water and temperature on long term mechanical behaviour of high performance concrete, 2nd Int. Symposium on Cement-based Materials for Nuclear Wastes, NUWCEM 2014, Avignon, France, 3-5 June 2014

[34] Alarcon-Ruiz, L, Platret, G, Massieu, E, Ehrlacher, A (2005) The Use of Thermal Analysis in Assessing the Effect of Temperature on a Cement Paste, Cement and Concrete Research, 35(3), pp. 609-613

[35] Di Luzio, G, Cusatis, G (2009a) Hygro-thermo-chemical modeling of high performance concrete. I: Theory, Cement and Concrete Composites, 31(5), pp. 301–308

[36] Di Luzio, G, Cusatis, G (2009b) Hygro-thermo-chemical modeling of high performance concrete. II: Numerical implementation, calibration, and validation, Cement and Concrete Composites, 31(5), pp. 309–324

[37] Ezziane, M, Molez, L, Jauberthie, R, Rangeard, D (2011) Heat-Exposure Tests on Various Types of Fibre Mortar, European Journal of Environmental and Civil Engineering, 15, pp. 715-726

[38] Nikoloutsopoulos, ND, Sotiropoulou, AB, Pandermarakis, ZG (2010) Fiber-Reinforced Cement Mortars Degradation after Their Exposure to Fire Conditions, EPJ Web of Conferences 6, 23001, DOI:10.1051/epjconf720100623001, 6 pp.

[39] Aydin, S, Yazici, H, Baradan, B (2008) High-temperature resistance of normal-strength and autoclaved high-strength mortars incorporating polypropylene and steel fibers, Construction and Building Materials, 22(4), pp. 504-512

[40] Dao, DV, Forth, JP (2013) Investigation of the Behaviour of Geopolymer Mortar after Heating to Elevated Temperatures, Proc. 3rd Int. Conf. on Sustainable Construction and Technologies, Kyoto (Japan), August 19-21, Paper T4-3, 9 pp.

[41] Menou, A, Mounajed, G, Boussa, A, Pineaud, H, Carré, H (2006) Residual Fracture Energy of Cement Paste Mortar and Concrete Subject to High Temperatures, Theoretical and Applied Fracture Mechanics, 45, pp. 64-71

[42] Bamonte, P, Gambarova, PG (2017) A Contribution to the Thermo-Mechanical Characterization of Cement Mortars at High Temperature, 2nd Int. Fire Safety Symposium – IFireSS 2017, Naples (Italy), June 7-9, pp. 241-248

[43] UNI EN 1015-11 (2007) Test Methods for Cementitious Mortars Suitable for Walls – Part 11: Determination of the Tensile Strength in Bending and of the Compressive Strength of the Mortar in the Hardened State, UNI - Italian Board for Standardization, Milan (Italy), 10 pp.

[44] Felicetti, R., Gambarova, P.G, (1998) Effects of high temperature on the residual compressive strength of high-strength siliceous concretes, ACI-Materials Journal, 95 (4), pp. 395-406

[45] ASTM C39 / C39M – 20 (2020) Standard test method for compressive strength of cylindrical concrete specimens. ASTM International, West Conshohocken, PA, 2020, www.astm.org, 8 pp.

[46] Eurocode 2 – EN 1992-1-2(2004) Design of Structures, Part 1-2: General Rules-Structural Fire Design, 2004, European Committee for Standardization, Brussels, Belgium.

[47] Tokyay, M., Özdemir, M. (1997) Specimen shape and size effect on the compressive strength of higher strength concrete, Cement and Concrete Research, 27(8), pp. 1281-1289

[48] Eurocode 2 – EN 1992-1-1(2004) Design of concrete structures – Part 1-1: General rules and rules for buildings, 2004, European Committee for Standardization, Brussels, Belgium.

[49] di Prisco, M., Felicetti, R., Gambarova, P. G., Failla, C. (2003) On the fire behavior of SFRC and SFRC structures in tension and bending, Proc. 4th Int. RILEM Workshop on High-Performance Fiber-Reinforced Cement Composites HPFRCC-4, ed. by A. E. Naaman and H. W. Reinhardt, Ann Arbor (MI, USA), pp. 205–220